Measured Radiation Behaviour of a UAV-attached LTE Antenna

Philipp Reingruber*, Robert Langwieser*, Taulant Berisha†, Christoph F. Mecklenbräuker*,
*Institute of Telecommunications, TU Wien, Vienna, Austria,
†Dimetor GmbH, Altenberg bei Linz, Austria

philipp.reingruber@tuwien.ac.at, robert.langwieser@tuwien.ac.at

***Abstract*—In wireless systems, the realised characteristics of antennas in their operational environment are of major interest. This is especially true for wireless remote-control systems in combination with unmanned aerial vehicles (UAVs). In this paper we discuss measurement-based evaluations of a commercially available multi-band long term evolution (LTE) antenna mounted to the fuselage of a UAV. In comparison to the same antenna operated without the UAV, we observe an impact on antenna impedance as well as shadowing effects caused by the geometry of the UAV. Both lead to a reduced performance of the antenna and subsequently a reduction in communication reliability and range may be expected.**

***Index Terms*—antennas, UAV, BVLOS, radiation, measurements.**

I. Introduction

Today, unmanned aerial vehicles (UAVs) are very popular in a multitude of scenarios and applications, like rescue and disaster operations [1] or as observation and measurement vehicle [2]. Future applications like parcel or food delivery are already under investigation. An overview on UAV bases applications can be found in [3][4].

UAVs of current applications as well as for future applications require reliable wireless communication for different purpose like flight control, real time video transmission or data download to name a few. Furthermore, over the horizon communication is a required and challenging task. In this context existing wireless infrastructure for mobile communication comes into focus for UAVs. This is especially true for beyond visual line of sight (BVLOS) communication between UAVs and UAV operators. For safe operation of UAVs in an integrated airspace, comprising both manned and unmanned aerial vehicles, reliable connectivity is safety critical. Even though cellular networks have not been built and optimized for aerial applications, the level of connectivity provided by long term evolution (LTE) has been demonstrated as sufficient for the lower airspace [5][6]. However, the communication performance the UAV experiences is very different from mobile subscribers at ground level. With increasing altitude, the number of signals received at the UAV originating from different base stations is increasing dramatically [5]. Furthermore, with the number of increasing neighbouring cells, the distance to the actual serving cells goes up significantly. This results in increased interference, increased latency and reduced handover quality.

Key components in such a scenario are of course antennas mounted on UAVs. Unfortunately, antenna parameters like radiation pattern, realized gain, and antenna impedance can change dramatically when mounted to a UAV compared to a free space environment. Understanding and optimizing the antenna characteristics at the UAV is a key issue for successful and safe drone flights via cellular networks.

In this paper we investigate experimentally the performance change of a commercially available multi-band LTE antenna when used in the proximity of a UAV fuselage. In Section II we give an overview on the investigated UAV and LTE antenna and in Section III we provide an explanation of our measurement setup and discuss our obtained results. Finally, in Section IV we conclude our paper.

II. UAV Configuration

A. UAV Description

The influence of the UAV model *SkyBee I* (shown in Fig. 1) on the performance of a user equipment (UE) LTE antenna was measured using the anechoic chamber of TU Wien. The wings and propellers were taken off in order to avoid collision with the probe antenna and to fulfil the minimum required distance of the spherical near-field system. Taking into account the proximity of the antenna to the fuselage shell, it can reasonably be assumed that the impact of the fuselage is of higher importance for the measurement than that of the wings and propellers.

The dimensions of the UAV fuselage are $130 \times 27 \times 40\ cm$ ($length \times width \times height$), with the width increased to $52\ cm$ on the lowest part of the UAV legs. Due to the size of the UAV, the radiation behaviour of the antenna was measured at LTE band 3 (at $1.8\ GHz$), band 2 (at $1.9\ GHz$), band 1 (at $2.1\ GHz$) and band 7 (at $2.6\ GHz$) [7, p. 45].

While the exact material composition of the fuselage shell is unknown, it can be stated that it consists of a composite of Glass Fibre Reinforced Plastic (GFRP) and Carbon Fibre Reinforced Polymer (CFRP). Based on [8], GFRP is expected to show lossy dielectric behaviour. According to [9], CFRP shows electromagnetic (EM) properties similiar to metals in the investigated frequency range. Depending on the layer

Fig. 1. UAV model *SkyBee I*, courtesy of Eurodragons GmbH, modified by the authors

composition of the CFRP, isotropy of these properties cannot be guaranteed.

B. LTE Antennas

Available specifications of the provided antenna are scarce, therefore we measured the required parameters. The UE LTE antenna, which is shown in Fig. 1, uses linear polarisation and has an input impedance of 50 Ω. This antenna is expected to work at multiple LTE frequencies. As shown in Fig. 1, the antenna is surrounded by a radome. It was connected to a coaxial cable via a SubMiniature version A (SMA) connector.

C. Mounting Positions

In order to determine the impact of the UAV on the antenna performance, measurements were performed in three different configurations: In the "stand-alone configuration", meaning the antenna was measured without being mounted on the UAV, and again when mounted in two predefined positions on the UAV.

The mounting position of the antenna visible in Fig. 2a is called "vertical configuration" as the antenna is in a vertical position when the UAV is in resting position. In this configuration, the feed point of the antenna is only centimetres away from the fuselage shell. Due to the shape of the shell, however, this physical distance increases at the lower parts of the bodywork with the tip of antenna being located below the fuselage.

The second mounting position of the LTE antenna visible in Fig. 2b is called "horizontal configuration". In this configuration, the antenna is in a horizontal position when the UAV is in resting position. Unlike in the vertical configuration, the entire antenna is in close proximity to the fuselage shell.

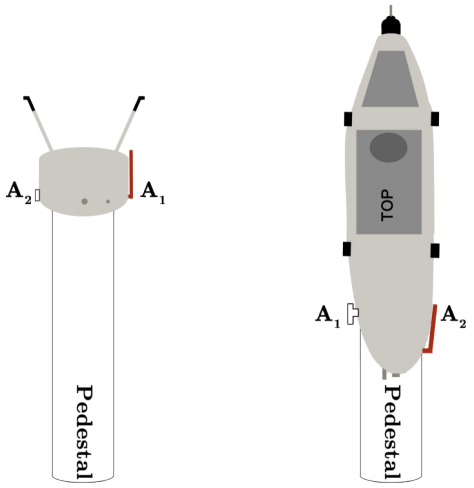

(a) View of vertical configuration at $\theta = 90°$ and $\varphi = 270°$

(b) View of horizontal configuration at $\theta = 90°$ and $\varphi = 270°$

Fig. 2. Antenna configurations; A_1 indicates the antenna in vertical configuration, A_2 indicates the antenna in horizontal configuration.

III. Measurement Setup and Results

A. Antenna Matching

Impedance matching over frequency of all three configurations shown in Fig. 3 was measured using a N9916A FieldFox Handheld Microwave Analyzer by Keysight Technologies. Performing the measurements of the reflection coefficient S_{11} are not subject to frequency limitations due to the antenna under test (AUT[1]) size; thus, LTE band 20 (at $0.8\ GHz$) [7, p. 45] is highlighted in the figure as well. The results of Fig. 3 are given in Tab. I for all observed LTE bands in a linear scale.

[1]The term *AUT* includes the entire measured object, e.g. the UAV.

Despite not providing distinct resonance frequencies at most LTE bands, the *stand-alone configuration* (including a sheath current filter) showed acceptable impedance matching. As stated in Tab. I, about 13 % of the power available to the antenna is reflected at frequencies of interest (corresponding to $S_{11} \approx -9\ dB$).

The dotted lines in Fig. 3 show the respective results of the antenna when being mounted on the UAV. Focusing on the results in *vertical configuration*, the UAV fuselage caused substantial change in impedance matching, but mostly outside the LTE bands. The reflection coefficient becomes more volatile with slightly higher peaks and deeper, albeit narrower minima. The resonance frequencies are shifted compared to the stand-alone configuration. Tab. I shows that the impedance matching at the LTE bands even marginally improves in this configuration.

Mounting the antenna in *horizontal configuration*, however, leads to a considerable deterioration of the results for all observed LTE bands with the exception of LTE band 7: At at LTE band 3, 2 and 1, about $\frac{1}{3}$ of the available power is reflected by the antenna structure; a portion that increases to more than $\frac{1}{2}$ at LTE band 20. It can be stated that significantly higher communication distances or less transmit power could be achieved in this configuration by adapting the impedance matching.

As the main difference between the UAV-including configurations is the distance between the antenna and the fuselage shell, it can be stated that optimised positioning including a higher gap to the fuselage has a beneficial effect on impedance matching.

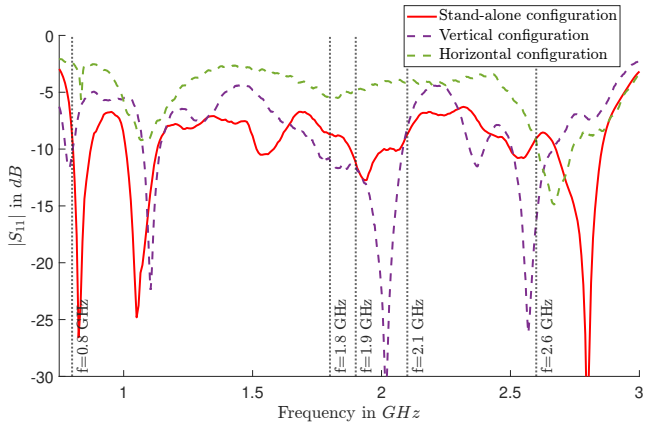

Fig. 3. Reflection coefficient comparison between stand-alone configuration and UAV-including configurations

TABLE I
REFLECTED PART OF AVAILABLE POWER IN ALL CONFIGURATIONS AT FREQUENCIES OF INTEREST

Frequency	Stand-alone	Vertical	Horizontal
0.8 GHz	13.06 %	9.46 %	57.8 %
1.8 GHz	13.40 %	8.05 %	29.3 %
1.9 GHz	7.57 %	7.03 %	31.3 %
2.1 GHz	13.49 %	15.38 %	38.6 %
2.6 GHz	12.39 %	2.37 %	11.5 %

B. Radiation Behaviour

1) Anechoic Chamber Setup: The anechoic chamber of TU Wien was used to measure the spatial distribution radiation behaviour of the AUT's radiation performance. The anechoic chamber provides a single gantry arm spherical near-field setup [10, p. 169] as shown in Fig. 4: The AUT is mounted on pedestals made of GFRP and/or Rohacell which are placed on an azimuth positioner. The probe antenna is mounted on a gantry arm placed above the AUT. The distance from the origin of coordinates to the probe antenna is 1.31 m. The arm rotates around the origin of coordinates and thus creates variation over the polar angle θ. Note that the gantry arm provides a limited motion around the θ-axis. Instead of rotating complete 180°, the rotation span is 160° to avoid collision with the pedestal. This limitation leads to the necessary assumption that the power density at $\theta > 160°$ is negligible in the radiating near-field region. The angle χ indicates the probe rotation angle used to adjust the polarisation of interest.

All configurations mentioned in Sec. II-C have a normalised initial orientation: At $\theta = 0°$, the aperture of the probe antenna was facing the tip of the antenna on the measured object. In order to achieve the consistent antenna orientation, the data obtained from the measurement in horizontal configuration (see Fig. 4) had to be flipped. The angle $\varphi = 0°$ indicates that the x-axis corresponded with the expected main beam direction, i.e. the axis of maximum radiation. The probe angle $\chi = 0°$ is used for co-polarisation. As a result, maximum

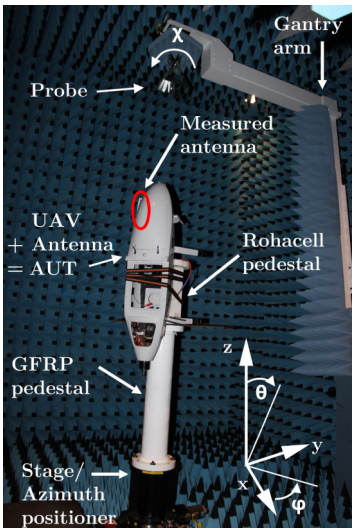

Fig. 4. Single gantry arm spherical near-field setup inside the anechoic chamber including the measurement coordinate systems

radiation values in case of a half-wave dipole would occur at $\theta = 90°$, $\varphi = 0°$, $\chi = 0°$. In order to detect cross-polarisation components, the measurement was repeated at $\chi = 90°$.

The near-field electric field strength was measured and converted to the far-field by the NSI 2000 Antenna Measurement System software. A theoretical description of near-field to far-field transformation techniques is given in [11, Ch. 17.2.4], while [12, Ch. 4.4] offers a practical explanation of the methods used by the measurement system.

2) Gain Patterns: The impedance matching and radiation behaviour of an antenna can be expressed using the realised gain ratio which compares the power density available to the antenna to the power density radiated in a certain direction [11, pp. 61–63][13]. Fig. 5 shows the spatial distribution of realised gain at all measured LTE bands for every configuration. As shown in the colour map on the right, shapes of red indicate areas of high gain while shapes of green and blue indicate areas of low gain.

The *stand-alone configuration* offers a half-wave dipole-like radiation behaviour: The radiated power density is distributed omnidirectionally along φ, the maximum *absolute* gain is close to 2.15 dBi and distinct nulls can be found at the tip and at the bottom of the antenna. Gain fluctuations along the θ-axis still occur, however, it is possible to mitigate them with a sheath current filter.

The radiation behaviour at $f = 2.6\ GHz$ is a clear exception to these dipole similarities: The variations over θ could not be sufficiently reduced, the directions of maximum gain are no longer located around $\theta = 90°$ but around $\theta \approx 60°$.

Mounting the antenna on the UAV in *vertical configuration* leads to a substantial change in the spatial gain distribution. As depicted in the second column of Fig. 5, the gain at lower frequencies is significantly reduced in regions where the UAV causes non-line-of-sight (NLOS) propagation (at $\varphi \in [90°, 270°]$). The fuselage in-between heavily attenuates

the signal in these directions. However, the electrical length of the gap between the LTE antenna and the fuselage grows with increasing frequency f as the wavelength λ decreases. Thus, the UAV-caused attenuation in these directions becomes smaller for higher frequencies.

An observation that occurs especially in NLOS directions is increased attenuation at higher θ-values ($\theta > 90°$). As stated in Sec. II-C, the gap between the fuselage shell and the antenna is larger at the lower parts of the bodywork, meaning at lower θ-angles. With the UAV in very close proximity, little power is transmitted through the obstacle at $\theta > 90°$, particularly for higher frequencies where the distance through the UAV is larger relative to the wavelength.

Especially in NLOS areas, where the physical distance to the UAV is short, meaning for $\theta > 90°$, higher gain values occur in regions where $\varphi > 180°$ (e.g. see Fig. 5h). The antenna is located on the front part of the UAV (at $\varphi > 180°$ in the vertical configuration). Thus, the signal travels a shorter distance through the UAV which results in less attenuation.

In line-of-sight (LOS) directions ($\varphi \in [0°, 90°]$ or $\varphi \in [270°, 360°]$) regions close to the tip and the bottom of the antenna ($\theta \approx 0°$ or $\theta \approx 180°$) are better covered at the lower LTE bands. The maximum gain remains similar to the stand-alone configuration. Small gain fluctuations occur both over θ and φ.

The *horizontal configuration* provides a maximum gain similar to the vertical configuration despite worse impedance matching described in Sec. III-A. However, due to the mounting position that offers a significant smaller gap to the fuselage shell, a multitude of limitations is caused by the UAV: The angle range where the realised gain is comparable to the maximum gain in stand-alone configuration is significantly smaller than in vertical configuration. Moreover, the NLOS areas are covered considerably worse with UAV-caused attenuation by more than 30dB for many directions.

Regions where $\theta < 90°$ are attenuated in particular. As $\theta < 90°$ represents the rear part of the UAV, like in vertical configuration, the gain depends on the distance the signal travelled through the UAV.

Compared to the other configurations, the gain pattern shows less variation over frequency; again with a noteworthy exception at $f = 2.6\ GHz$ where the pattern is again characterised by gain fluctuations: While the gain in NLOS directions is less attenuated, there is no homogeneous LOS region of constant high gain, e.g. when the aperture of the probe antenna is facing the expected beam axis of the AUT ($\theta = 90°, \varphi = 0°$), the realised gain is only $-10.7\ dBi$.

3) Polarisation: In order to quantify the polarisation purity, the cross-polarisation discrimination (XPD) is calculated. Note that the colour map is adjusted for Fig. 6 which exemplarily depicts the spatial distribution of XPD for every configuration at $f = 2.1\ GHz$: Positive values represented by red shades show a dominating co-pol gain, while negative values represented by blue shades show a dominating cross-pol gain. Green areas show similar gains in both polarisations.

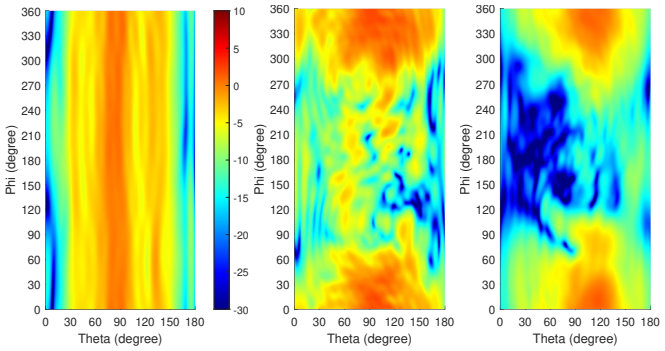

(a) Stand-alone configuration at 1.8 GHz (b) Vertical configuration at 1.8 GHz (c) Horizontal configuration at 1.8 GHz

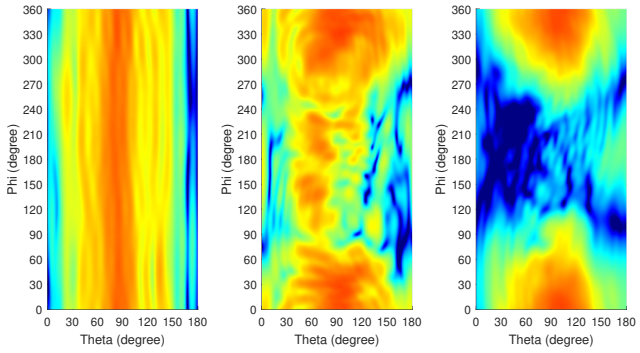

(d) Stand-alone configuration at 1.9 GHz (e) Vertical configuration at 1.9 GHz (f) Horizontal configuration at 1.9 GHz

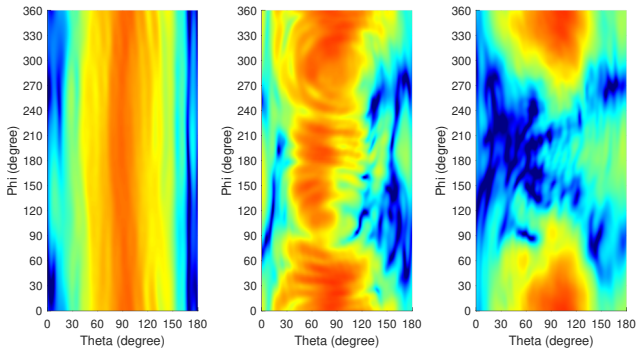

(g) Stand-alone configuration at 2.1 GHz (h) Vertical configuration at 2.1 GHz (i) Horizontal configuration at 2.1 GHz

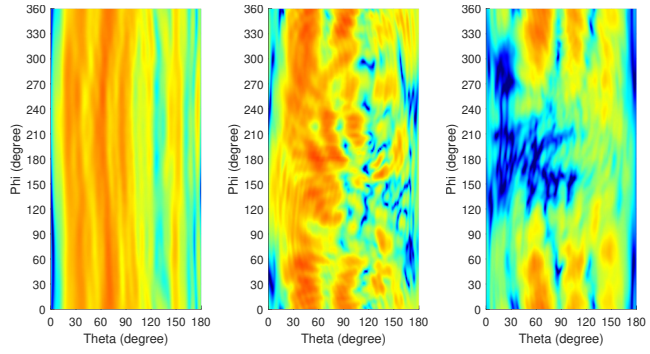

(j) Stand-alone configuration at 2.6 GHz (k) Vertical configuration at 2.6 GHz (l) Horizontal configuration at 2.6 GHz

Fig. 5. Spatial distribution of realised gain G_{re} (co-pol). The colour bar in Fig. 5a indicates gain values in dBi for all plots.

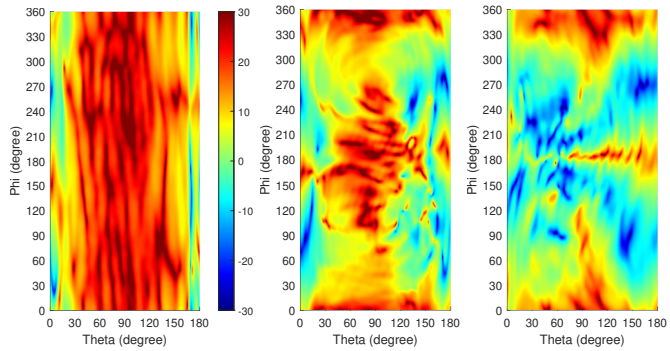

(a) Stand-alone configuration (b) Vertical configuration (c) Horizontal configuration

Fig. 6. Spatial distribution of cross-polarisation discrimination XPD at 2.1 GHz. The colour bar in Fig. 6a indicates gain values in dB for all plots.

As indicated in Fig. 6a, power radiated in cross-polarisation is negligible for this antenna in *stand-alone configuration*. Only close to the tip and at the bottom of the antenna (at $\theta < 30°$ or $\theta > 165°$) where distinct co-pol gain nulls occur, the cross-pol gain is comparable or higher than the co-pol gain.

Fig. 6b and Fig. 6c highlight that the UAV impacts polarisation as well. In *vertical configuration*, the co-pol gain exceeds the cross-pol gain in central LOS and NLOS regions ($\varphi \approx 0°$ or $\varphi \approx 180°$) by more than 30 dB in some directions. The cross-pol gain becomes relevant when approaching the limits between LOS and NLOS ($\varphi \approx 90°$ or $\varphi \approx 270°$) when the signal travels along the fuselage shell. This suggests that EM excitation of the fuselage shell, which would lead to radiating currents, occurs.

In case of the *horizontal configuration*, the co-pol gain only outperforms the cross-pol gain in central LOS regions ($\varphi \approx 0°$), and in small areas at $\theta \approx 90°$ and at $\varphi \approx 180°$.

At $f = 2.6$ GHz, the XPD figures for the UAV-including configurations show that in vertical configuration, most power is radiated in co-polarisation except for very low ($\theta < 15°$) and high θ-angles ($\theta > 120°$). In case of the horizontal configuration, the cross-pol gain is similar to the co-pol gain once the probe antenna is positioned outside of $\varphi \approx 0°$ and $\varphi \approx 180°$.

IV. Conclusion

In this paper, the impact of a UAV on impedance matching and radiation behaviour of a UAV-mounted UE LTE antenna was analysed. In stand-alone configuration, the antenna offers acceptable impedance matching and half-wave dipole-like radiation behaviour for LTE bands 3, 2 and 1. The UAV causes significant attenuation and depolarisation effects in NLOS directions, i.e. the omnidirectional radiation behaviour gets lost. In LOS directions, the gain improves only slightly, which suggests that the UAV deteriorates the overall antenna performance. The impact of the UAV depends on three main reasons: The distance between the mounted antenna and the UAV and the distance that the signal has to travel through or along the UAV influence the attenuation and depolarisation caused by the UAV. The signal frequency also had an effect on the antenna performance; in particular, gain fluctuations at 2.6 GHz might cause communication reliability issues.

This work allows a more comprehensive understanding of antenna performance in the vicinity of a UAV. Furthermore, these results will help enabling enhanced antenna management, reducing the negative effects for drone operations at altitudes way above average cell tower height.

Acknowledgment

The authors want to thank Eurodragons GmbH for their support to this work, especially for providing the UAV.

References

[1] S. Waharte and N. Trigoni, "Supporting Search and Rescue Operations with UAVs," 2010 International Conference on Emerging Security Technologies, 2010, pp. 142-147, doi: 10.1109/EST.2010.31.

[2] A. Y. Umeyama, J. L. Salazar-Cerreno and C. J. Fulton, "UAV-Based Far-Field Antenna Pattern Measurement Method for Polarimetric Weather Radars: Simulation and Error Analysis," in IEEE Access, vol. 8, pp. 191124-191137, 2020, doi: 10.1109/ACCESS.2020.3027790.

[3] H. Shakhatreh et al., "Unmanned Aerial Vehicles (UAVs): A Survey on Civil Applications and Key Research Challenges," in IEEE Access, vol. 7, pp. 48572-48634, 2019, doi: 10.1109/ACCESS.2019.2909530.

[4] S. Mugala, D. Okello and J. Serugunda, "Unmanned Aerial Vehicles: Opportunities for Developing Countries and Challenges," 2020 IST-Africa Conference (IST-Africa), 2020, pp. 1-10.

[5] Qualcomm Inc., "LTE Unmanned Aircraft Systems, Trial Report, v1.0.1." 2017. https://www.qualcomm.com/documents/lte-unmanned-aircraft-systems-trial-report

[6] M. Nekrasov et al., "Evaluating LTE Coverage and Quality from an Unmanned Aircraft System," 2019 IEEE 16th International Conference on Mobile Ad Hoc and Sensor Systems (MASS), 2019, pp. 171-179, doi: 10.1109/MASS.2019.00029.

[7] 3rd Generation Partnership Project, "TS 36.101: Evolved Universal Terrestrial Radio Access (E-UTRA); User Equipment (UE) radio transmission and reception. V17.3.0." October 1st, 2021. https://www.3gpp.org/ftp/Specs/archive/36_series/36.101/36101-h30.zip , online.

[8] D. Asprone, D. Assante, A. Chiariello, G. Manfredi, G. Miano, A. Prota, and G. Rubinacci, "Assessment of the electromagnetic disturbance of a glass fiber reinforced composite fencing structure," *Journal of Composites for Construction*, vol. 14, no. 5, pp. 629–635, 2010. doi: 10.1061/(asce)cc.1943-5614.0000121.

[9] G. Artner, R. Langwieser, and C. F. Mecklenbräuker, "Carbon fiber reinforced polymer as antenna ground plane material up to 10 GHz," in *2017 11th European Conference on Antennas and Propagation (EUCAP)*, pp. 3601–3605, IEEE, 2017. doi: 10.23919/eucap.2017.7928128.

[10] J. Hald, J. E. Hansen, F. Jensen, and F. Holm Larsen, *Spherical Near-field Antenna Measurements*. IEE electromagnetic waves series, London, U.K.: The Institution of Engineering and Technology, 1988. doi: 10.1049/PBEW026E.

[11] C. A. Balanis, *Antenna Theory*. Hoboken, NJ, USA: Wiley, 4th ed., 2016.

[12] G. Masters, K. Haner, and J. Demas, *NSI 2000 (Near-field Edition), Version 4, Software Operating Manual, Revision F (SOM-NSI2000-V4, Rev F)*. NSI-MI Technologies, Torrance, CA, USA, 2011. Available: Institute of Telecommunications, Technische Universität Wien.

[13] "IEEE standard for definitions of terms for antennas," *IEEE Std 145-2013 (Revision of IEEE Std 145-1993)*, pp. 1–50, 2014. doi: 10.1109/IEEESTD.2014.6758443.